Biomaterials 32 (2011) 7870–7882

Contents lists available at ScienceDirect

Biomaterials

journal homepage: www.elsevier.com/locate/biomaterials

The pro-myogenic environment provided by whole organ scale acellular scaffolds from skeletal muscle

Barbara Perniconi [a,c], Alessandra Costa [a,b,2], Paola Aulino [a], Laura Teodori [b,*], Sergio Adamo [a,1], Dario Coletti [a,c,1]

[a] Sapienza University of Rome, Department of Anatomical, Histological, Forensic & Orthopaedic Sciences, Histology & Medical Embryology Section, 00161 Rome, Italy
[b] Diagnostics and Metrology Laboratory, UTAPRAD-DIM, ENEA-Frascati, 00044 Rome, Italy
[c] UPMC Univ Paris 6 – UR4, F-75005 Paris, France

ARTICLE INFO

Article history:
Received 4 July 2011
Accepted 5 July 2011
Available online 30 July 2011

Keywords:
ECM (extracellular matrix)
In vivo test
Muscle
Stem cell

ABSTRACT

In the pursuit of a transplantable construct for the replacement of large skeletal muscle defects arising from traumatic or pathological conditions, several attempts have been made to obtain a highly oriented, vascularized and functional skeletal muscle. Acellular scaffolds derived from organ decellularization are promising, widely used biomaterials for tissue engineering. However, the acellular skeletal muscle extra cellular matrix (ECM) has been poorly characterized in terms of production, storage and host–donor interactions. We have produced acellular scaffolds at the whole organ scale from various skeletal muscles explanted from mice. The acellular scaffolds conserve chemical and architectural features of the tissue of origin, including the vascular bed. Scaffolds can be sterilely stored for weeks at +4 °C or +37 °C in tissue culture grade conditions. When transplanted in wt mice, the grafts are stable for several weeks, whilst being colonized by inflammatory and stem cells. We demonstrate that the acellular scaffold *per se* represents a pro-myogenic environment supporting *de novo* formation of muscle fibers, likely derived from host cells with myogenic potential. Myogenesis within the implant is enhanced by immunosuppressive treatment. Our work highlights the fundamental role of this niche in tissue engineering application and unveils the clinical potential of allografts based on decellularized tissue for regenerative medicine.

1. Introduction

A hallmark of biomaterials, an evolving concept recently reviewed by Williams [1], is the *in vivo* interaction with the host's biological components. The various strategies used to obtain biomaterials for tissue engineering (TE) applications include allografts produced by the recellularization of previously decellularized tissues. Such allografts are widely used, especially for *in vivo* replacement of tissues and organs whose spatial organization and biochemical composition are complex. The decellularization of an explanted tissue can be achieved through various approaches, all of which eliminate the cellular compartment and leave a spatially and chemically preserved ECM [2]. These approaches have been successfully used to produce transplantable vessels, skin and cardiac tissues [3–5]. The ECM is, by definition, nature's ideal biological scaffold material. Indeed, it is specifically synthesized by the resident cells of each tissue and is obviously biocompatible since host cells produce their own matrix. The ECM also provides a supportive medium for blood or lymphatic vessels and for nerves. As reviewed in detail by Badylak, the ECM possesses all of the characteristics of the ideal tissue-engineered scaffold or biomaterial [6]. However, since complex three-dimensional organization of the structural and functional molecules that make up the ECM has not yet been fully characterized, synthesis of this material cannot be fully reproduced in the laboratory. ECM can be obtained from allogenic or syngenic donors, which may pose the histocompatibility and resorption problems that are typical of allografts. ECM scaffold materials that are resistant to degradation appear to elicit a pro-inflammatory macrophage (M1)-like response, whereas the anti-inflammatory (M2) macrophage phenotype prevails in native ECM scaffold materials, which are consequently readily degraded [7].

* Corresponding author. Tel.: +39 0694005642.
E-mail address: laura.teodori@enea.it (L. Teodori).
[1] Contributed equally to this work.
[2] 2010 Student Award of the International Society for the Advancement of Cytometry.

0142-9612/$ – see front matter © 2011 Elsevier Ltd. All rights reserved.
doi:10.1016/j.biomaterials.2011.07.016

Recent advances in skeletal muscle TE have opened new perspectives for the replacement of this tissue in common clinical applications, such as traumatic injury, extended tissue ablation or denervation [8]. Key issues in skeletal muscle TE are the composition and architecture of the ECM of this tissue, which is characterized by a highly ordered and hierarchical organization of muscle fibers. Several attempts have been made to address this issue by seeding fibrillar matrices with myoblasts or myogenic stem cells [8]. Skeletal muscle constructs have been obtained by using the ECM deriving from decellularized tissue. In particular, acellular muscles have been used by Borschel et al. as a substratum for C2C12 myoblast cultures, thus producing constructs capable of longitudinal contractile force upon electrical stimulation [9]. The same authors have obtained vascularized constructs by culturing C2C12 cells in a fibrinogen hydrogel contained within cylindrical silicone chambers and transplanting them around the femoral vessels in isogeneic adult recipient rats [9]. Patches of homologous muscle acellular matrix seeded with autologous myoblasts have been used to repair abdominal wall defects in rodents [10]. Minced muscle replaced in its bed has been shown to effectively regenerate fibers, though such fibers are spatially disorganized probably owing to the loss of ECM spatial orientation [11]. ECM and growth factors deeply affect various aspects of cell behavior, including survival, proliferation and differentiation, and are therefore key issues in TE applications [12]. In both pathological conditions, such as Duchenne's muscular dystrophy, and healthy conditions, such as after strenuous exercise, skeletal muscle tissue is maintained and repaired through regeneration [13]. As regeneration is strongly influenced by ECM and growth factors, ECM extracts have been used to coat culture dishes to induce muscle differentiation *in vitro* [14]. The role of growth factors in muscle regeneration has also been investigated in depth both *in vitro* and *in vivo* [15–17]. In order to promote host–donor tissue integration and vascularization, engineered factor VIII-releasing synthetic fibers have been used as a scaffold for myoblast cell culture before transplantation of the constructs into murine recipients [18].

While the generation of a whole functional, bioengineered rodent heart has demonstrated that it is possible to produce highly complex whole organs *in vitro* [5], a functional, anatomically defined skeletal muscle transplantable *in vivo* has not yet been produced. Few studies have evaluated and characterized the host immune response to non-autologous ECM scaffold materials. To this purpose, we generated an acellular scaffold from skeletal muscle and transplanted it into syngeneic hosts. This approach allowed us to extensively characterize histocompatibility, bioactivity and integration of acellular scaffolds in a murine model.

2. Materials and methods

2.1. Animals

Adult sex-matched BALB/C mice were used throughout this study as both donors and hosts. For specific experiments, adult nude athymic mice (strain NU/NU Crl:NU-Foxn1nu, Charles River, Milano, Italy) were used. Mice were treated according to the guidelines of the Institutional Animal Care and Use Committee. Donor animals were sacrificed before skeletal muscle removal, while host animals were anesthetized before muscle dissection and replacement with the acellular scaffold. The transplantation procedure is described in detail below. Immunosuppressive treatment consisted of 1 μl/g body weight of a 100 mg/ml Cyclosporin A (CSA) solution in peanut oil injected i.p., as previously described [19]. Vehicle was used for controls.

2.2. Decellularization of skeletal muscle

Freshly dissected *Tibialis anterior* (TA) and *Extensor digitorum longus* (EDL) were immediately incubated in sterile 1% SDS in distilled water respectively for 24 and 48 h, at RT under slow rotation. At least 10 ml of SDS solution was used for each pair of muscles. At the end of the decellularization procedure, the muscles were thoroughly washed by means of 3 incubations lasting 30 min each in sterile PBS. Decellularized scaffolds were used on the same day as they were produced or were stored for specific experiments.

2.3. Experimental design and surgical procedure

TA acellular scaffolds were used to replace TA of inbred, age- and sex-matched wt mice, unless otherwise indicated. The grafts were subsequently dissected from the host one, two, three and four weeks following transplantation. The production of an adequate number of acellular scaffolds was planned according to the surgical procedures. Following anesthesia with Avertin A (tribromoethanol and 2-methilbutanol from Sigma–Aldrich, St Louis, MO, USA), the skin over the left TA was sterilized and the hair removed. An incision was created in the skin layer and the dermal flap opened to expose the TA epimisium, which was in turn carefully lifted on one side to allow dissection of the underlying TA. The distal tendon and a small fragment of the muscle inserted proximally on the tibia were left in place as substrata for suturing the grafted material. The acellular scaffold was properly oriented and sutured with silk thread (USP 5-0 TR-17 black silk 45 cm). The scaffold was then covered by the epimisium, and the latter sutured with silk thread. Lastly, the skin flap was used to cover the wound and closed with 3–4 stitches of silk thread (USP 3-0 TT-26 black silk 45 cm). The filmed surgical procedure is included in Supplementary material.

2.4. Histological and histochemical analysis

The TA was dissected, embedded in tissue freezing medium (Leica, Wetzlar, Germany) and frozen in liquid nitrogen-cooled isopentane. Cryosections (8 μm, unless otherwise specified) were obtained from the mid-belly of the graft using a Leica cryostat. For histological analysis, the sections were stained with hematoxylin and eosin using standard methods and Masson's trichrome staining kits (Sigma).

Esterase staining was adapted from Davis [20] as previously reported [21]: cryosections of each muscle were incubated for 5 min in a staining solution containing: 3 mg alpha-naphthyl acetate, 0.375 ml acetone, 6.25 ml 0.2 M sodium phosphate and 0.4 ml of a solution containing equal volumes of 2% pararosaniline (Sigma) and 2% sodium nitrite. Photomicrographs were obtained using an Axioscop 2 plus system equipped with an Axiocam HRc (Zeiss, Oberkochen, Germany) at 1300 × 1030 pixel resolution.

2.5. Immunofluorescence analysis

Transverse cryosections were fixed in 4% paraformaldehyde for 10 min at room temperature. After incubation with 1% BSA (Sigma) for 30 min, the samples were incubated with a 1:100 dilution in 1% BSA of polyclonal anti-laminin or anti-fibronectin Ab (Sigma), followed by incubation with 0.5 ug/ml Hoechst 33342 (Sigma). A 1:500 dilution in BSA of anti-mouse-Alexa 488 Ab was used to detect endogenous IgG on cryosections of the grafted material, while a 1:500 dilution in BSA of anti-rabbit-Alexa 488 or anti-rabbit-Alexa 568 Ab was used to detect the polyclonal anti-laminin or anti-fibronectin Abs above. An aliquot of 25,000 cells from flow cytometry experiments was cytocentrifuged and used for the immunofluorescence analysis. To detect PW1 (recently highlighted as a stem cell marker that specifically identifies stem cells with myogenic potential [22,23]) expression, we used a 1:2000 dilution in 1% BSA of a polyclonal anti-PW1 custom-made Ab, followed by incubation with a 1:500 dilution in 1% BSA of anti-rabbit-Alexa 568 (Molecular Probes, Eugene, OR, USA). Pre-immune serum was used for the negative control. Hoechst was used as above to counterstain cell nuclei. Photomicrographs were obtained by means of an Axioskop 2 plus system (Zeiss) or a Leica Leitz DMRB microscope fitted with a DFC300FX camera for confocal analysis (Leica).

2.6. Dot blot analysis

Three types of samples were analyzed with this approach: freshly prepared acellular scaffolds, acellular scaffolds stored for two weeks at +4 °C in PBS, and acellular scaffolds stored for two weeks at +37 °C (in a 5% CO_2 atmosphere) in DMEM. For each type of sample, four scaffolds were pooled and homogenized in 320 μl of Laemli sample buffer. For each sample, 1–4 μl were then spotted on a nitrocellulose membrane. The aspecific binding sites were blocked with 5% milk in TBST for 30 min. The membrane was rinsed for 5 min with TBST and incubated with Rabbit anti-laminin antibody (Sigma) diluted 1:1000 in 5% BSA/TBST for 30 min at RT. The membrane was then rinsed 3 times, for 5 min each, in TBST and incubated it with HRP goat anti-rabbit antibody (Biorad) diluted 1:10000 in 1% milk in TBST for 30 min at RT. Following extensive rinsing in TBST, ECL was developed with Super signal west Pico chemiluminescent substrate (Pierce).

2.7. Flow cytometric analysis

The graft, the contralateral TA and a TA from a healthy mouse that did not undergo surgery were separately dissected, minced and digested in a solution containing 50 U/ml type II collagenase (Sigma), 35 U/ml type IV hyaluronidase (Sigma) and 1 mg/ml collagenase/dispase in phosphate buffered solution (PBS) for

1 h at 37 °C, as previously reported [21]. Following serum addition (to inhibit digestion), the slurry was filtered through a 40 um strainer, centrifuged and resuspended in PBS. The cells were fixed in 2% paraformaldehyde for 10 min, incubated with 1% BSA for 30 min, followed by a 1:100 dilution in 0.1% BSA of PE-Cy5-conjugated anti-CD45 monoclonal Ab or of FITC-conjugated anti-Sca-1 monoclonal Ab for 30 min at room temperature (BD Biosciences, San Jose, CA, USA). Isotype Abs were used for setting auto- and aspecific fluorescence. Additional antibodies used in CD45+ cells bivariate analyses (all used at a final concentration of 0.025 μg/μl) were: M3/84 rat anti-mouse Mac3 and RB6-8C5 rat anti-mouse Ly-6G/Gr-1 to detect macrophages and granulocytes (neutrophils and eosinophils), respectively (BD Biosciences); rat anti-mouse CD3 for identifying T cells. To distinguish cells from ECM debris, we counterstained the cells with 50 μg/ml PI solution. The cells were washed and suspended in 0.1% BSA, and analyses were performed on a Coulter Epics XL flow cytometer (Beckman Coulter, Fullerton, CA, USA). At least 100,000 events were recorded and data were analyzed with the Summit (Beckman Coulter) software. Gating strategy: PI positive cells were gated and plotted in a biparametric variable dot plot showing cell forward (FSC) and side (SSC) scatter. According to the background settings, CD45 or Sca-1 positive cells were gated and represented in the corresponding dot plots. For each sample 20,000 cells were assessed. The percentage of CD45 or Sca-1 positive cells in replicate experiments was averaged and statistically compared.

3. Results

3.1. Acellular scaffold generation from skeletal muscle

A protocol based on a sequence of incubations in iso-osmotic and then hyposmotic detergent solutions was proposed some years ago to make acellular EDL muscle scaffolds from adult mice [9]. More recently, it has been shown that incubation in 1% SDS in deionized water completely decellularizes a whole murine heart [5]. We applied the latter method to two murine skeletal muscles, the EDL and the TA, which differ above all on account of the disparity in the size of their masses, which are 10 and 40 mg, respectively [24]. We collected muscles from sacrificed mice and immediately proceeded to decellularization. Following SDS treatment, the muscles appeared translucent and dilated, probably owing to the absence of cell–cell and cell–matrix constraints, retaining their shape and a stiff consistency (Fig. 1A). Since our method differed significantly from those previously published regarding skeletal muscle, in a preliminary experiment we used morphological criteria to assess the minimum time required to achieve complete decellularization as a function of the muscle mass. We found that the optimal incubation time in SDS was 24 h and 48 h for the EDL and the TA, respectively (Fig. 1B). Since the morphology of the two muscles appeared similar following decellularization, the TA was chosen and used throughout our study for practical reasons. The latter was further analyzed by SDS-PAGE electrophoresis, in order to assess how the decellularization process affected the protein composition of the samples. A freshly collected TA was compared to an acellular scaffold and to the supernatant of the acellular scaffold following the process of decellularization, by Coomassie Blue staining of the gel (Suppl. Fig. 1). In agreement with a previous report [14], we showed the extraction of a large number of proteins present in the skeletal muscle (i.e. their presence in the supernatant and absence in the acellular scaffold). However, the acellular scaffold contained several high molecular weight (>75 kDa) proteins, which exhibited a nearly identical banding pattern as compared to the naïve muscle (Suppl. Fig. 1).

In hematoxylin and eosin (H&E) stained cross-cryosections, the acellular scaffold appeared as a faintly stained network of filamentous material reminiscent of the endomysial organization

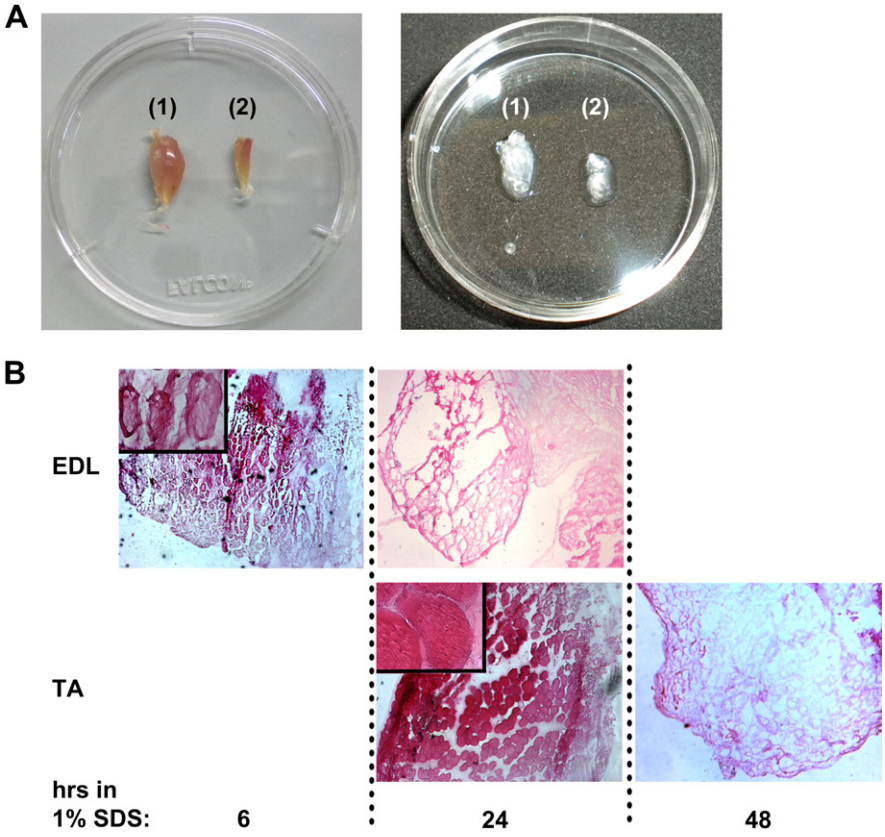

Fig. 1. Decellularization of whole mouse muscles. A) Macroscopic appearance of the (1) *Tibialis anterior* (TA) and the (2) *Extensor digitorum longus* (EDL) before (left panel) and after (right panel) decellularization. B) H&E stained cryosections of the TA and EDL showing the kinetics of decellularization: the EDL and TA display the persistence of myofibers (insets) following incubation of 6 h and 24 h, respectively, in 1% SDS in deionized water, while 24 h and 48 h, respectively, were sufficient to achieve complete decellularization.

typical of the control muscle (i.e. a matching non-decellularized muscle); the pink staining observed after decellularization pointed to the nature of the material (i.e. protein), while purple nuclei and eosinophil fibrillar material were absent, contrasting sharply with the control (Fig. 2A). The persistence of the ECM fibrillar components following decellularization was further highlighted by Masson's trichrome staining, which showed the complete loss of cellular compartments in the presence of conserved ECM (Fig. 2B). In addition, Fig. 2B shows that the ECM matrix surrounding the vessels was preserved, thus demonstrating not only that the ECM organization specific to muscle tissue was maintained, but that the whole organ ECM network was likely to have been preserved. To assay the extent of the decellularization procedure, we specifically detected molecular components of either the cellular or the ECM compartments. By phalloidin and Hoechst DNA staining, we demonstrated the complete loss of both cell microfibrillar actin and nuclei, respectively (Fig. 2C). Following decellularization, two ECM components, i.e. laminin and fibronectin, were not only retained, but they preserved the polygonal organization that is typical of the cross-section resulting from the naïve architecture of the basal lamina (Fig. 2D and E).

To verify in detail whether the spatial organization of the basal lamina was preserved following the chemical and mechanical stress it was subjected to, during preparation of the acellular scaffold, we performed an immunofluorescence confocal analysis, followed by 3D reconstruction of serial images obtained from laminin staining of acellular scaffold cryosections (Fig. 3A). The basal lamina conserved a polyhedral tubular organization that corresponded to the spaces previously occupied by individual muscle fibers. These spaces varied in size, likely mirroring the former presence of fiber populations of varying sizes, which are physiologically present in the TA (Fig. 3A).

Since a major goal of TE is the generation of off-the-shelf constructs ready to be transplanted, we assessed whether acellular scaffolds could be stored over time. We thus stored freshly produced acellular scaffolds for two weeks in sterile conditions at either +4 °C in PBS (Fig. 3B) or +37 °C (in a 5% CO_2 atmosphere) in DMEM (Fig. 3C). At the end of the two weeks, neither the presence of laminin nor the architecture were affected, suggesting that the acellular scaffold we produced can be stored not only at low temperatures, but even in cell culture grade conditions. To quantitatively assess whether ECM proteins are affected by a two-week storage, we choose to measure the amount of a specific protein, i.e. laminin, as a marker of proteolysis during storage. First, we performed a dot blot for laminin on extracts obtained from freshly produced acellular scaffolds, and acellular scaffolds that were stored for two weeks at either +4 °C in PBS or +37 °C (in a 5% CO_2 atmosphere) in DMEM. As indicated in Fig. 3D, we spotted different amounts of each sample which gave rise to proportionally increased signals, demonstrating the linear response of the assay. With this approach, we noticed that the storage at +4 °C in PBS had a minor impact on the amount of laminin in acellular scaffolds, while the storage at +37 °C in DMEM diminished by about 50% the amount of laminin as compared to the storage at +4 °C in PBS (Fig. 3D). It is worth to recall, though, that laminin architecture did not seem to be affected in spite of the proteolysis occurring at +37 °C (Fig. 3C and D). To further assess this critical issue, we also performed laminin quantification by a morphometric analysis of quantitative fluorescence data. To validate this approach, we spotted on glass different amounts of a standard, purified laminin and we recorded fluorescence intensity following IF fluorescence analysis; we could demonstrate a linear correlation between the amount of laminin and the fluorescence signal for a wide range of fluorescence intensities (Suppl. Fig. 2A and B). Within this range, we recorded immunofluorescence images of

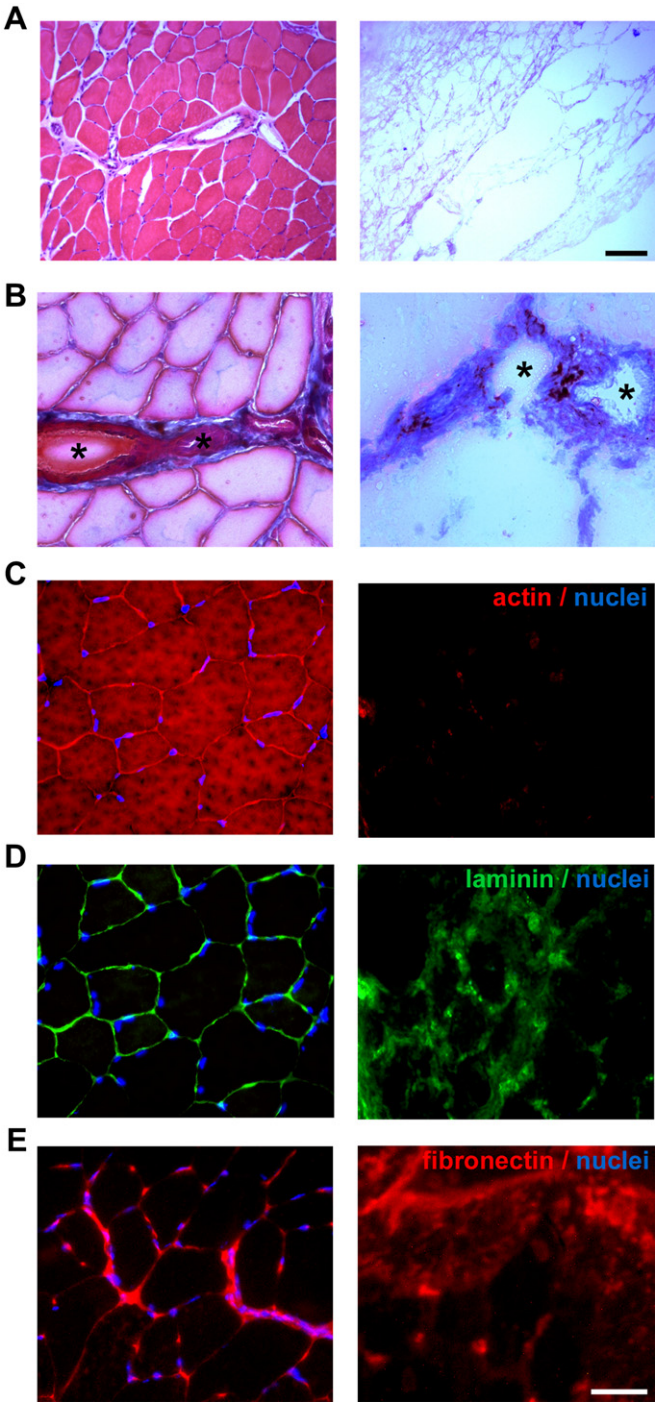

Fig. 2. Composition and characteristics of decellularized skeletal muscle. Skeletal muscle cryosections were analyzed before (left) and after (right) decellularization: A) H&E staining showing the loss of eosinophil sarcomeric material and hematoxylinophil nuclei and the conservation of filamentous protein material. B) Masson's trichrome staining showing no intact cells or nuclei in the SDS-treated muscle in the presence of preserved ECM filaments and large vasculature conduits (a vein and an artery in this microscopy image, black asterisks). C) Immunofluorescence micrographs depicting the loss of Hoechst (blue) staining of intact nuclei as well of folloidin (red) staining of sarcomeric actin. D) and E) Immunofluorescence micrographs showing that the ECM components laminin (green) and fibronectin (red) were, unlike the nuclei (blue), preserved. Fluorescence intensity appears to increase in decellularized muscle images, presumably owing to the decompression of the matrix following the removal of cells, but the overall circular organization in cross-sections is preserved. Scale bars, 50 μm. (For interpretation of the references to colour in this figure legend, the reader is referred to the web version of this article.)

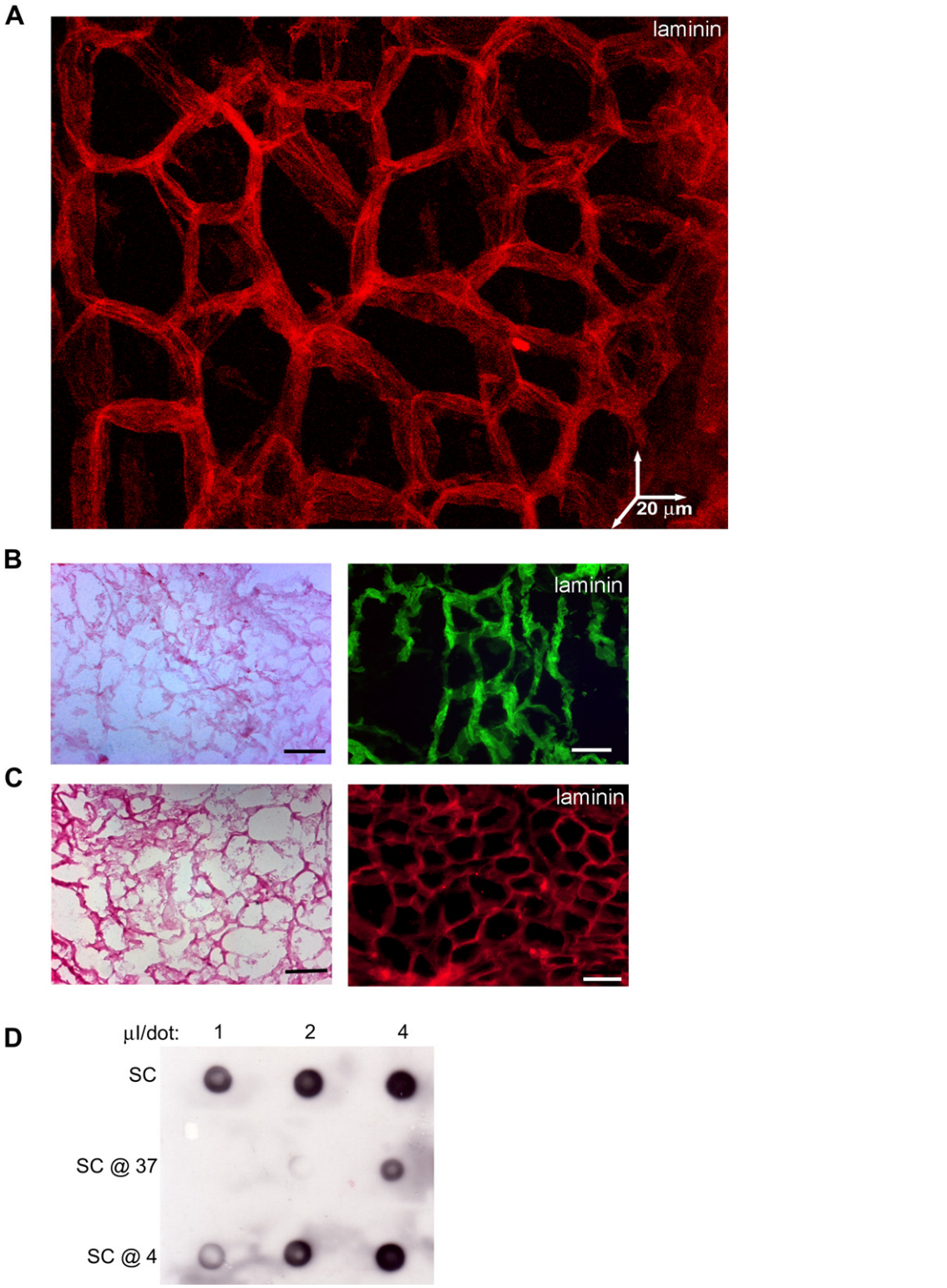

Fig. 3. Acellular skeletal muscle scaffolds maintain the 3D-architecture and can be stored. A) 3D image stack reconstruction of confocal microscopy images of a 20 μm thick cryosection of acellular skeletal muscle scaffold, following laminin immunodetection (red). The latter highlights the irregular, polyhedral tubular organization corresponding to that of the muscle fibers. B) H&E (left panel) and immunofluorescence (right panel) staining for laminin (green) of acellular scaffold after two weeks of storage in sterile PBS at +4 °C. Laminin expression and architecture is maintained in this condition. Scale bar, 50 μm. C) H&E (left panel) and immunofluorescence (right panel) staining for laminin (red) of acellular scaffold after two weeks of storage in sterile DMEM in a cell culture incubator at +37 °C. Laminin expression and architecture is maintained in this condition, suggesting that acellular muscle scaffold can be used for cell culture. Scale bar, 50 μm. C) Representative image of dot blot analysis of laminin content. Freshly prepared scaffold (SC), acellular scaffold after two weeks of storage in sterile DMEM at +37 °C (SC@37) or acellular scaffold after two weeks of storage in sterile PBS at +4 °C (SC@4) were solubilized in equal volumes of buffer and the indicated amount spotted on a nitrocellulose membrane on which a WB for laminin was performed. The ECL signal is proportional to the spotted amount of ECM laminin for each sample, and highlights quantitative differences in laminin content due to storage conditions. (For interpretation of the references to colour in this figure legend, the reader is referred to the web version of this article.)

Table 1
Quantification of laminin in basement membrane of muscle and scaffolds.

Sample	Fluorescence intensity (% ctrl)
Muscle	100 ± 8
Scaffold	95 ± 4
Scaffold @ 4 °C	91 ± 10
Scaffold @ 37 °C	53 ± 5*

Shown is the mean fluorescence intensity ± SEM of laminin immunostaining on cross-cryosections expressed as % of control (i.e. Tibialis muscle, TA). Sampled materials were: freshly isolated TA, freshly produced acellular scaffold, acellular scaffold stored for 2 weeks in PBS at +4 °C, and acellular scaffold stored for 2 weeks in DMEM at +37 °C. *$p < 0.01$ by Student's t test, $n = 8$.

laminin in cross-sections of naïve TA muscle, freshly prepared acellular scaffold and scaffold stored at either +4 °C or +37 °C for two weeks. On these images, we performed quantitative analysis of the plot profile along an axis randomly chosen for any microscopic field (Suppl. Fig. 2C). As shown by the plots of fluorescence intensity as a function of the analyzed pixel for the four different sample types, the signal for laminin in the basement membrane consistently appeared as repetitive peaks at a distance of about 50 μm from each other in all the samples (Suppl. Fig. 2D). Nonetheless, the average peak integral of each sample varied, as reported in Table 1, showing that the acellular scaffold have an amount of laminin similar to the naïve skeletal muscle, and that they lose about 10% and 50% of laminin following storage at +4 °C or +37 °C for two weeks, respectively.

3.2. Inflammatory response to acellular scaffolds

In order to test the interaction between the skeletal muscle acellular scaffold and the host, acellular scaffolds were orthotopically transplanted in mice. For this purpose, the left TA was removed and immediately replaced with a skeletal muscle acellular scaffold obtained from the TA of a matching BALB/c mouse (i.e. an animal from the same breeding). The detailed procedure can be seen in the movie included in Supplementary material (Suppl. data movie). Briefly, the acellular scaffold was sutured distally, by joining the host tendon to the tendon fragment of the acellular scaffold, and proximally, by using a small fragment of endogenous TA muscle inserted in the proximity of the joint to serve as an attachment for the silk thread. Particular care was used to retain the host epimysium, which was used to cover the graft and was then held in place by a stitch. Lastly, the skin flap was re-positioned to cover the implant and sutured using standard procedures. This method allowed us to identify three regions in the graft (Suppl. Fig. 3), henceforth referred to as proximal (i.e. near the a proximal suture knot), mid-belly (i.e. within the central region, characterized by the maximal thickness of the construct) and distal (i.e. toward the distal suture knot on the tendon). Unless otherwise stated, the mid-belly region was analyzed at least 1000 μm from the proximal suture knot.

Movie S4.

We initially sectioned grafted materials after two weeks *in vivo*. Nuclear staining of the sections showed that the graft was entirely colonized by cells, which invaded the space both within and around the basal lamina (Fig. 4A). Anti-Ig antibody positivity, which was observed in this context, revealed the occurrence of overt inflammation (Fig. 4A). To clarify the nature of the infiltrating cells, we enzymatically extracted the cells from the graft and performed a flow cytometry analysis for CD45+ cells (Fig. 4B). We found that these cells were abundant within the graft, which was in sharp contrast to the contralateral TA muscle of the host, which displayed a CD45 population similar to that detectable in the TA muscle of a healthy, non-transplanted animal (Fig. 4B and C). These findings indicate that an abundant leukocytic population invades the graft and that inflammation is restricted to the grafted material. Experiments performed four weeks after transplantation showed that the degree of inflammation had decreased toward control levels (Fig. 4C). We further investigated inflammation by fluorometric analysis of cell-specific inflammatory markers co-expressed by the CD45+ cells, including CD3 for lymphocytes, GRA1 for granulocytes and MAC3 for macrophages. By biparametric analysis we could demonstrate that CD45+ are mostly represented by macrophages, even though granulocytes and T lymphocytes are also present in the musculature of mice (Table 2). The relative abundance of these CD45 sub-populations is not altered in the contralateral TA muscle of the host, while the graft appears to be enriched in granulocytes both at two and four weeks following transplantation (Table 2). Given the relevance of macrophage invasion to ECM remodeling and skeletal muscle regeneration, we also assessed the presence of this specific subpopulation of CD45+ cells in the grafts by esterase staining. We found a massive presence of these cells two weeks following transplantation, which is likely to account, at least in part, for the afore-mentioned CD45+ population (Fig. 4D).

Injuring muscle in healthy untransplanted animals results in an inflammatory reaction that is readily followed by repair mediated by satellite cells, or other stem cells, thereby giving rise to myofiber neoformation. Thus, we scored the presence of potentially myogenic stem cells by flow cytometry analysis of enzymatically extracted cell preparations from grafts of TA muscles. On the basis of the differential FSC and SSC properties, we found two stem cell antigen-1 (Sca-1) positive populations in the graft two weeks after transplantation (Fig. 5A). The population with lower FSC and SSC was also found in both the contralateral muscle and in control muscle from non-operated animals (Fig. 5A). Sca-1 *per se* is a rather aspecific stem cell antigen; in skeletal muscle, Sca-1 is co-expressed with PW1/Peg3, which has recently been identified as a pivotal marker for stemness that is expressed in muscle interstitial stem cells and has been named PICs [22,23]. We confirmed the presence of PICs in the grafted material by assessing the cellular expression of the specific marker PW1 [22] cytocentrifuged preparations of these samples (Fig. 5B).

3.3. Acellular scaffold myogenic potential

Immunofluorescence analysis of graft cross-cryosections one week following transplantation revealed that the laminin presence and architecture were conserved in spite of the massive infiltrate (Fig. 6A). Morphological analysis revealed the striking presence of nascent myofibers scattered throughout the inflammatory cell population (Fig. 6B). These muscle fibers varied in size but were significantly bigger than the surrounding cells and displayed

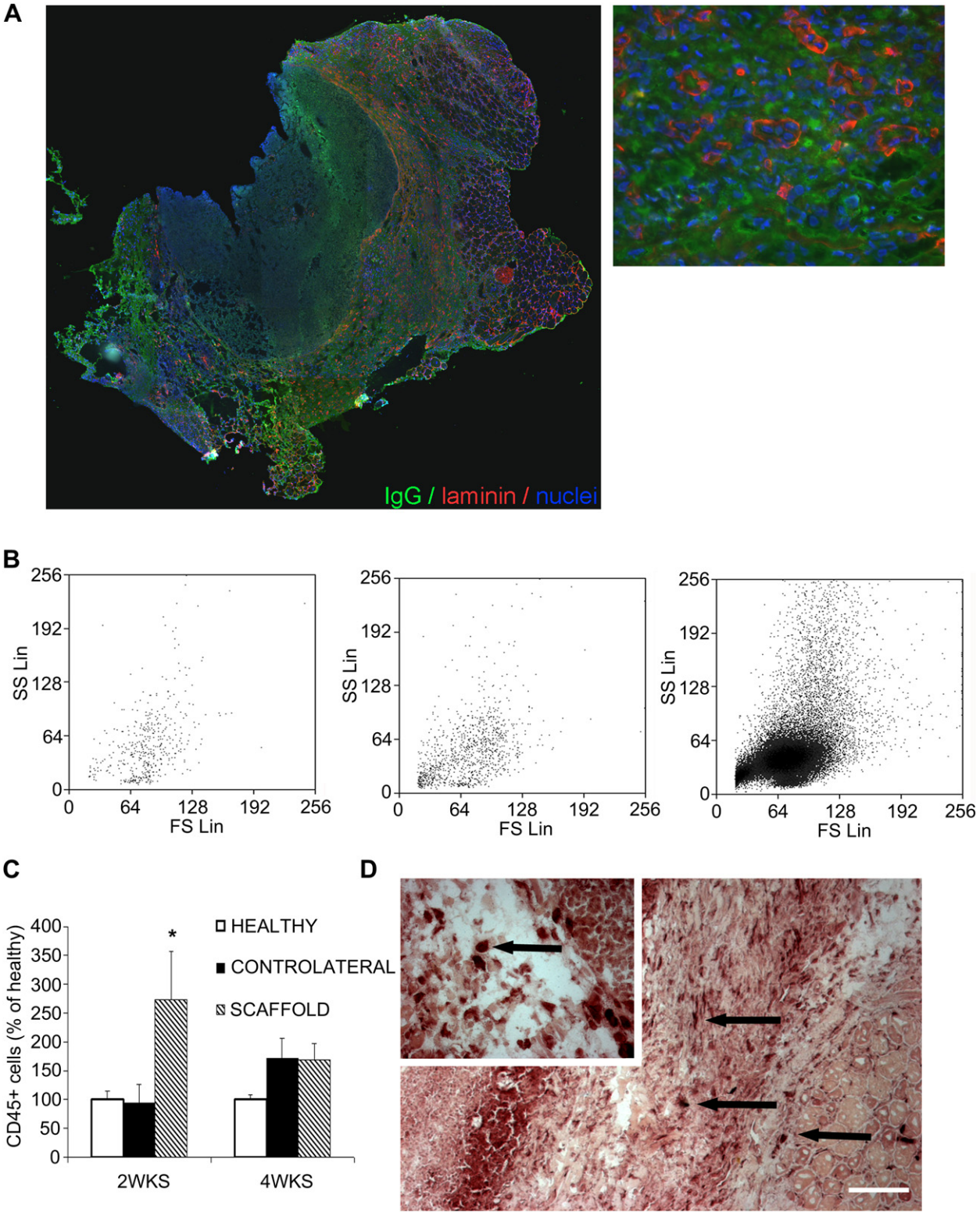

Fig. 4. Grafted scaffolds are invaded by immune cells. A) Left panel, immunofluorescence analysis of a whole graft cross-section two weeks after transplantation. Right panel, higher magnification of a specific region. The graft is completely invaded by cells, whose nuclei are stained by Hoechst (blue), entering and surrounding the scaffold laminin (red) in the presence of mouse G immunoglobulins (green). B) Biparametric flow cytometry analysis shows cell forward (FSC) and side scatter (SSC) of CD45 expressing cells extracted from: i) a TA muscle of a healthy, non-operated mouse (left panel), ii) a contralateral TA muscle of a host mouse (middle panel) and iii) grafted scaffold (right panel) two weeks after transplantation. C) Quantification of the CD45 expressing cells in triplicate experiments as in B at the one- and four-week time points. Cell numbers are expressed as fold induction over non-operated controls. $^{*}p < 0.05$ by Student's t test. The presence of inflammatory cells progressively returns to control levels. D) Esterase staining on graft cryosection two weeks after transplantation demonstrates the presence of macrophages (arrows) within the muscle ECM implant. The inset represents a micrograph at higher magnification/resolution obtained with a 40× lens. Scale bar, 100 μm. (For interpretation of the references to colour in this figure legend, the reader is referred to the web version of this article.)

Table 2
Quantification of sub-populations in CD45+ cells (%).

	2 Weeks			4 Weeks		
	CD3	GRA1	MAC3	CD3	GRA1	MAC3
Healthy	4 ± 2	10 ± 4	24 ± 8	–	–	–
Contralateral	3 ± 1	8 ± 3	35 ± 2	2 ± 2	9 ± 2	33 ± 4
Scaffold	14 ± 3	48 ± 6	20 ± 9	6 ± 1	43 ± 10	35 ± 2

Flow cytometric analysis of CD45 expressing cells extracted from: TA muscle of a healthy, non-operated mouse (Healthy), contralateral TA muscle of a host mouse (Contralateral), and grafted scaffold (Scaffold) two and four weeks following transplantation. A biparametric analysis was performed for CD45 and lymphocyte (CD3), granulocyte (GRA1), or macrophage (MAC3) markers. The mean percentage of CD45 expressing cells co-expressing the indicated markers is shown ±SEM; $4 < n < 8$ for each subpopulation analyzed.

abundant eosinophil cytoplasms and centrally located nuclei, two hallmarks of skeletal muscle regenerating fibers. The regenerating fibers were located far from the host muscle, either in a radial or longitudinal direction, throughout the graft (Fig. 6B). Two weeks after transplantation, the appearance of the grafted material was still characterized by the presence of a number of scattered regenerating muscle fibers and mononuclear cells (Fig. 6C). The expression of muscle-specific proteins, such as Myosin Heavy Chain and Sarcoglycan, demonstrated the presence of *bona fide* muscle fibers in this region (Fig. 6D).

Since we detected an abundant population of CD45 expressing cells in the grafts, suggesting leukocytes were involved in the graft–host interactions, we exploited athymic nude mice as recipients for wt acellular TA scaffolds in transplantation experiments. Two weeks after transplantation, we confirmed the generation of skeletal muscle fibers in the grafted material by both morphological and molecular analysis (Fig. 7A and B). In particular, the expression of muscle specific, late differentiation markers demonstrated the presence of newly formed skeletal muscle tissue; moreover, the number of myofibers did not appear to be altered significantly in immuno-depressed animals (Fig. 7B). To better mimic the clinical settings, in parallel experiments we treated the hosts with CSA, a commonly used immunosuppressor [25,26], and compared the results with those obtained in vehicle-treated hosts. Within this context, we extended our analysis to three and four weeks post-transplantation. As shown in Fig. 8, we found that the myofibers survived up to four weeks following transplantation in control conditions and that they localized preferentially at the mid-belly (Fig. 8A and B) and proximal regions of the grafts (data not shown). We also noted that the mid-belly of the graft in CSA-treated animals was rich in newly formed muscle fibers, which were also present, though to a lesser extent, in the distal region (Fig. 8A and B).

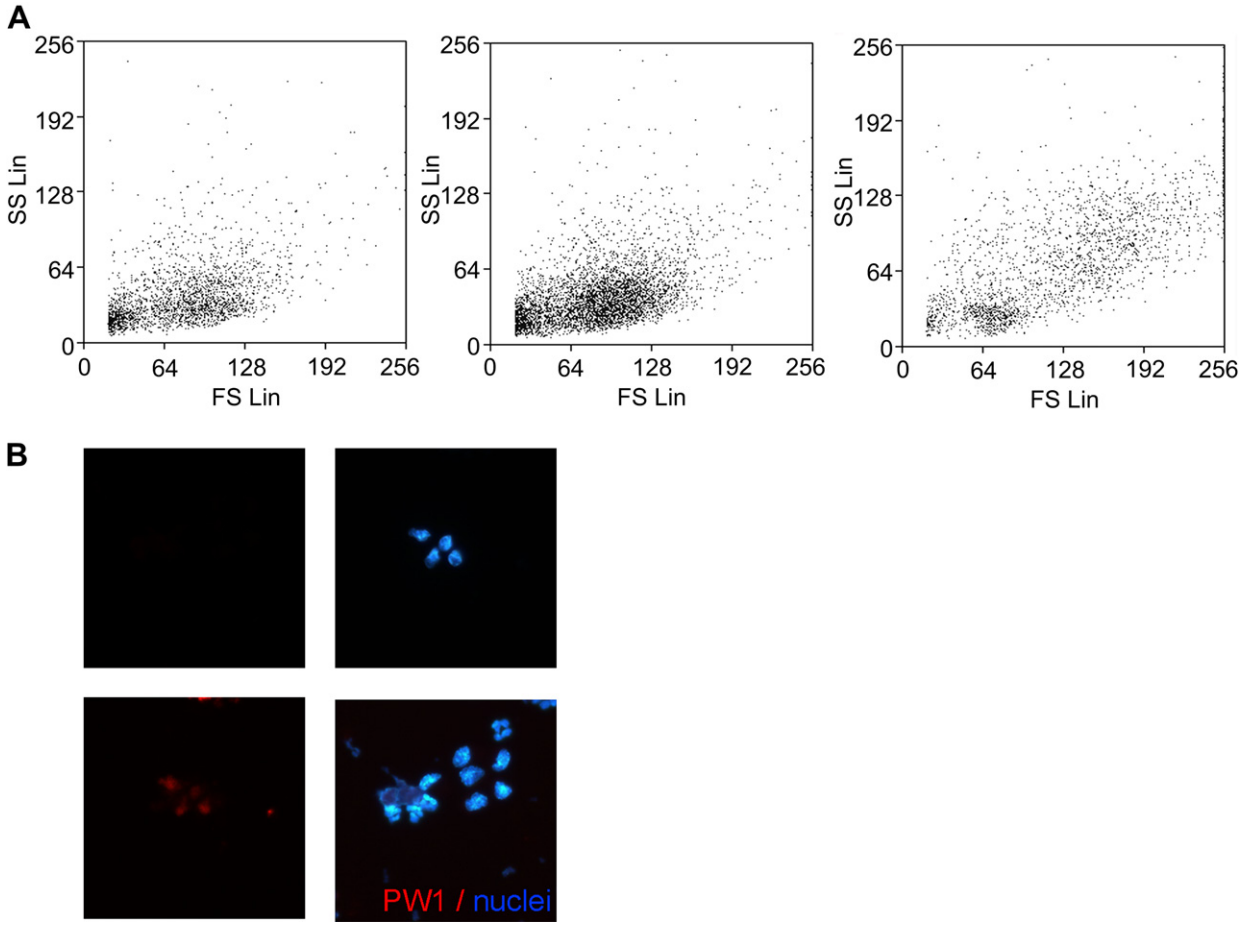

Fig. 5. Muscle stem cells are recruited by the grafted scaffold. Biparametric flow cytometry analysis shows cell forward (FSC) and side scatter (SSC) of stem cell antigen-1 (Sca-1) expressing cells extracted from: i) a TA muscle of a healthy, non-operated mouse (left panel), ii) a contralateral TA muscle of a host mouse (middle panel) and iii) grafted scaffold (right panel) two weeks following transplantation. The FSC and SSC analysis shows that at least two populations of Sca-1 expressing cells are detectable in the muscle ECM implant. Sca-1 expression points to stem cell recruitment. B) Cytocentrifuged cells from the preparation above were subjected to immunofluorescence analysis for PW1 (red), a specific marker for muscle interstitial stem cells. Cells recruited by the graft and counterstained with Hoechst (blue) express PW1 (upper panels). Lower panels represent a negative control for the immunostaining, i.e. cells incubated with pre-immune serum as primary Ab. (For interpretation of the references to colour in this figure legend, the reader is referred to the web version of this article.)

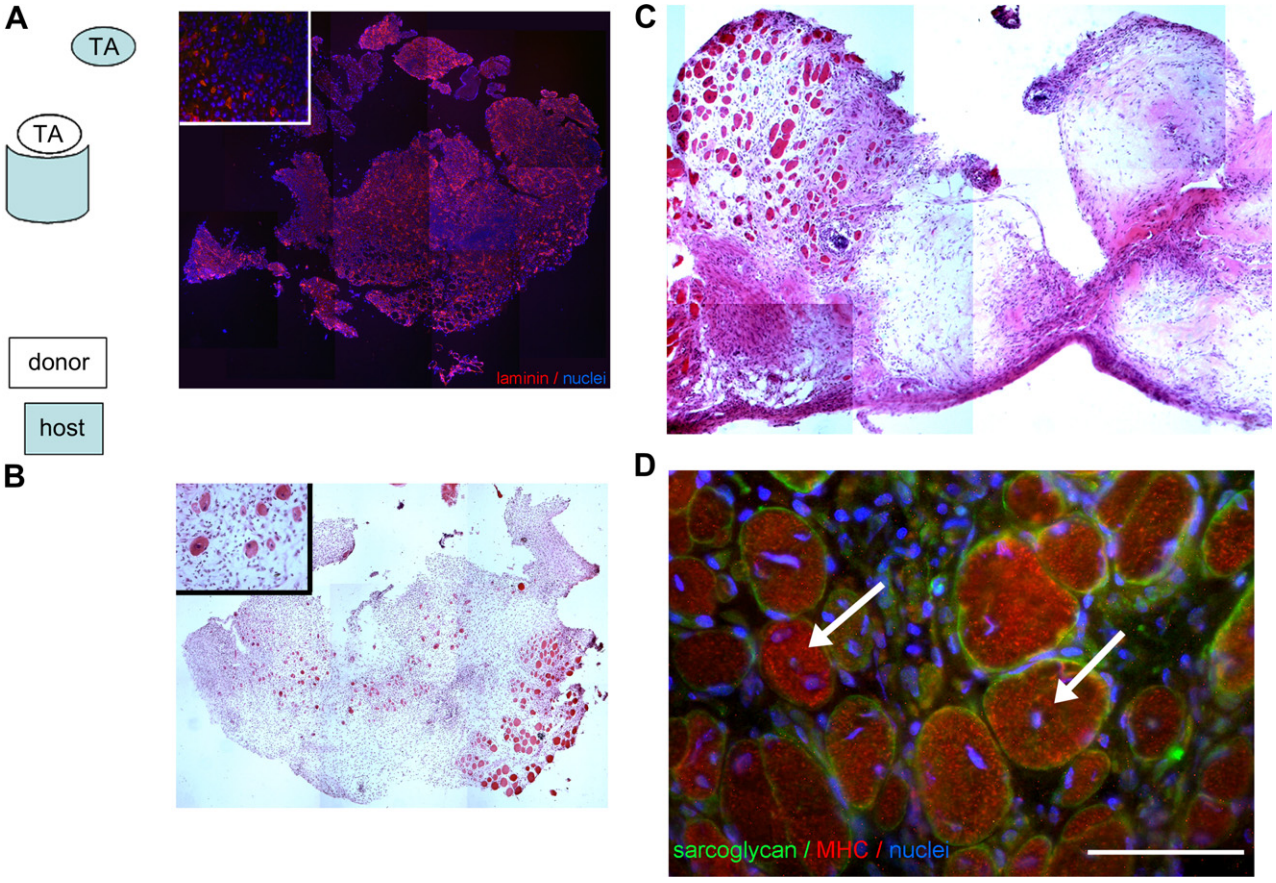

Fig. 6. Host–donor tissue integration. The diagram depicts the experimental procedure, consisting in host TA (blue) removal, followed by orthotopic transplantation of a TA acellular scaffold (white). Reconstruction of a whole graft cryosection at the mid-belly at the one-week (A and B) and two-week (C and D) time points, obtained by merging a series of high definition images of immunofluorescence (A and D) or H&E (B and C) stained samples. In A the laminin (red) and Hoeschst (blue) stainings show the persistence of the basal lamina architecture and the presence of an abundant population of infiltrating cells. Panel B highlights the presence of nascent myofibers characterized by abundant eosinophil cytoplasm and centrally located nuclei. The insets show 20× magnification of the image. The environment composed of transplanted ECM sustains myogenesis despite significant inflammation. C) Graft histology one week later demonstrates the persistence of regenerating fibers and the mononucleated cell population. D) Immunofluorescence analysis of muscle-specific molecular markers highlights the expression of Fast-Myosin Heavy Chain (red) and Sarcoglycan (green) in myofibers with centrally located nuclei (blue), thereby demonstrating that these cells (arrows) are generating *bona fide* skeletal muscle tissue. Bar = 50 μm. (For interpretation of the references to colour in this figure legend, the reader is referred to the web version of this article.)

4. Discussion

An increasing amount of interest is being expressed in tissue engineering and regenerative medicine as a means of restoring or replacing lost or malfunctioning tissues and organs through the use of cells and biomaterial scaffolds [27]. Adopting a widely used approach, either autologous or heterologous cells are cultured in a biocompatible three-dimensional porous scaffold supplemented with growth factors to regenerate new tissues or organs. The scaffold provides necessary interim support for cell adhesion, proliferation and differentiation; moreover, it offers the biochemical and biophysical cues required to modulate the *de novo* tissue formation by mimicking the functional and structural characteristics of the native ECM, which plays a crucial role in controlling and regulating cell behavior and function [28]. The results achieved in the TE of skeletal muscle are lagging behind those achieved for other tissues types owing to the complexity of the former. Major issues in skeletal muscle TE are: i) the marked abundance of this tissue, which represents roughly 40% of the body mass, and the relatively large size of most of the muscles; ii) hierarchical and complex three-dimensional organization in parallel bundles of muscle tissue surrounded by connective tissue and other tissue types; iii) capillary vascularization required for survival; iv) innervation for functional performance *in vivo*; v) tendinous connection with bone for the mechanical musculoskeletal interaction. We believe, as do Taylor and co-workers [5], that using nature's platform to engineer an organ is a rational approach to address the afore-mentioned issues, which are shared by both cardiac and skeletal muscle tissue. Thus, we adapted the technique developed for cardiac muscle to skeletal muscle in an attempt to generate whole organ scaffolds, consisting of the ECM of a whole acellular muscle. The muscle retains the distal tendon attached to one extremity and conserves its morphology and stiffness, including intact arterial and venous basement membranes, in the absence of endogenous cells. The first method designed to obtain skeletal muscle decellularization dates back to the early 1990s [29]. That method, as well as more recent ones, are based on long, specific series of enzymatic and detergent treatments aimed at selectively eliminating any trace of cellular constituents, i.e. intracellular proteins, nucleic acids and lipids [6]. If compared with these previously published methods, our method is simpler (one passage), faster (one or two days) and guarantees sterility (since both prokaryotic and eukaryotic cells are lysed by SDS). The scaffolds obtained by this method can be stored for a few weeks at +4 °C, since the preservation of laminin amount and 3D organization suggests that the ECM is well preserved; worth noting, in

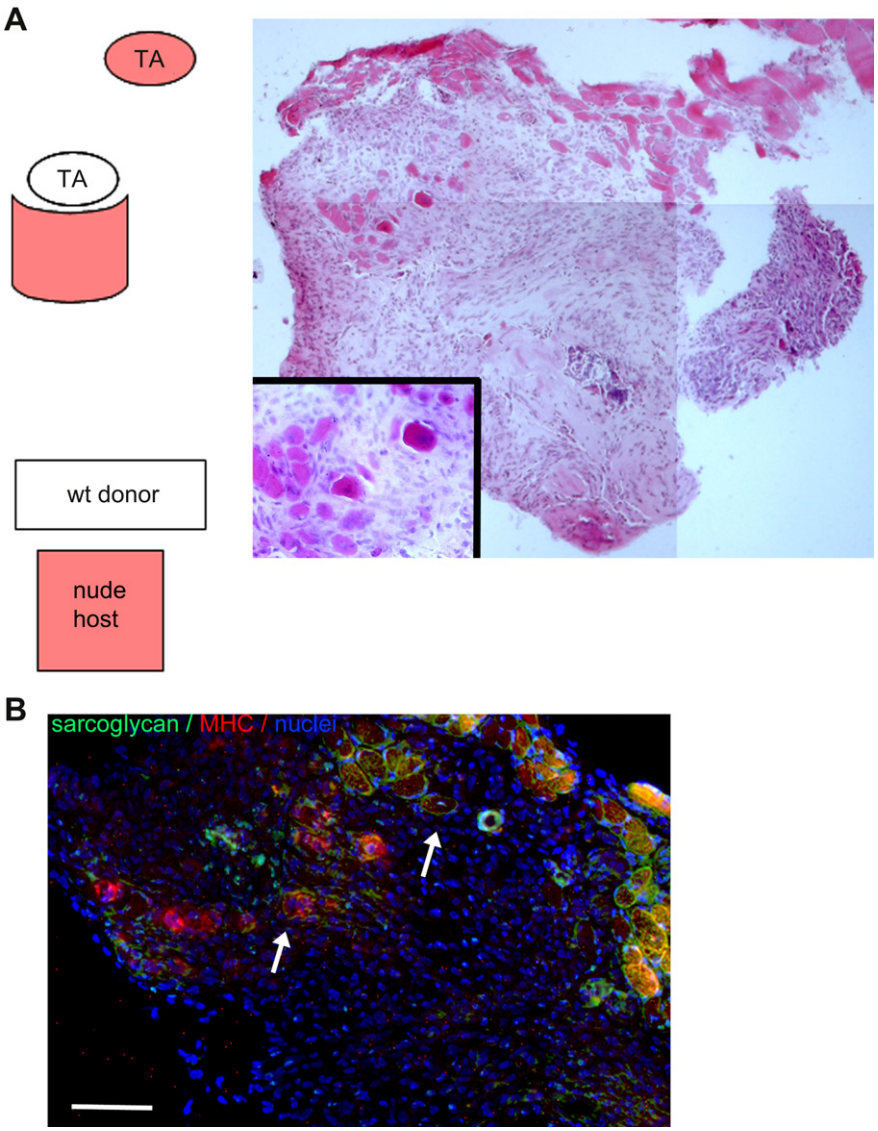

Fig. 7. Host–donor tissue integration in transgenic nude mice. The diagram depicts the experimental procedure, consisting in host TA (red) removal, followed by orthotopic transplantation of a TA acellular scaffold (white). Reconstruction of a whole graft cryosection at the mid-belly at the two-week time point, obtained by merging of a series of high definition images of a representative H&E stained sample. Panel A highlights the presence of nascent myofibers characterized by abundant eosinophil cytoplasm and centrally located nuclei). The inset shows 20× magnification of the image. B) Immunofluorescence analysis of muscle-specific molecular markers highlights the expression of Fast-Myosin Heavy Chain (red) and Sarcoglycan (green) in myofibers with centrally located nuclei (blue), demonstrating that these cells (arrows) are generating *bona fide* skeletal muscle tissue. Bar = 50 μm. In the absence of differentiated T lymphocytes (due to the athymic phenotype of nude mice, which hampers lymphocyte maturation), both the inflammatory and the myogenic populations appear to be unaffected, as the histology resembling that of wt mice at the same time point suggests. Thus, lymphocyte do not appears to play a major role in inflammation and remodeling. (For interpretation of the references to colour in this figure legend, the reader is referred to the web version of this article.)

tissue culture grade conditions a significant proteolysis occurs, even though overall laminin organization appears to be maintained.

Although the use of a biological scaffold is shared by all these methods, the host immune response to these materials and the effect of the immune response upon downstream remodeling events has remained largely unexplored [30]. Conjugating histocompatibility with availability of the starting material is one of the main goals of transplantation-based regenerative medicine interventions. This issue is particularly relevant to skeletal muscle, since autografts may not be possible if more than a certain amount of tissue is required. On the other hand, allografts induce morbidity at the donor site and adverse inflammatory reactions in the host. Although it has been suggested that ECM is less immunogenic than whole tissues [31], the addition of cells to the ECM scaffold has been shown to reduce the inflammatory response upon grafting [32]. In an attempt to shed light on these contrasting results, we transplanted acellular scaffolds from wt mice into wt hosts of an inbred strain, which may mimic a clinical setting of transplant between histocompatible individuals. Our results revealed a significant immune response, of which macrophages are a major component. It has been reported that about 60% of the mass of ECM scaffold materials is degraded and resorbed within four weeks of transplantation (reviewed by Ref. [30]). However, the degradation of an ECM scaffold may be a requisite process with bioactive consequences that contribute to the overall remodeling events. Low molecular weight peptides formed during the degradation of ECM scaffolds have displayed chemoattractant potential for several cell types *in vitro*, including multipotent progenitor cells [33]. We noted a reduction in the grafted material four weeks after transplantation (data not shown) and cannot exclude that the persistence of the

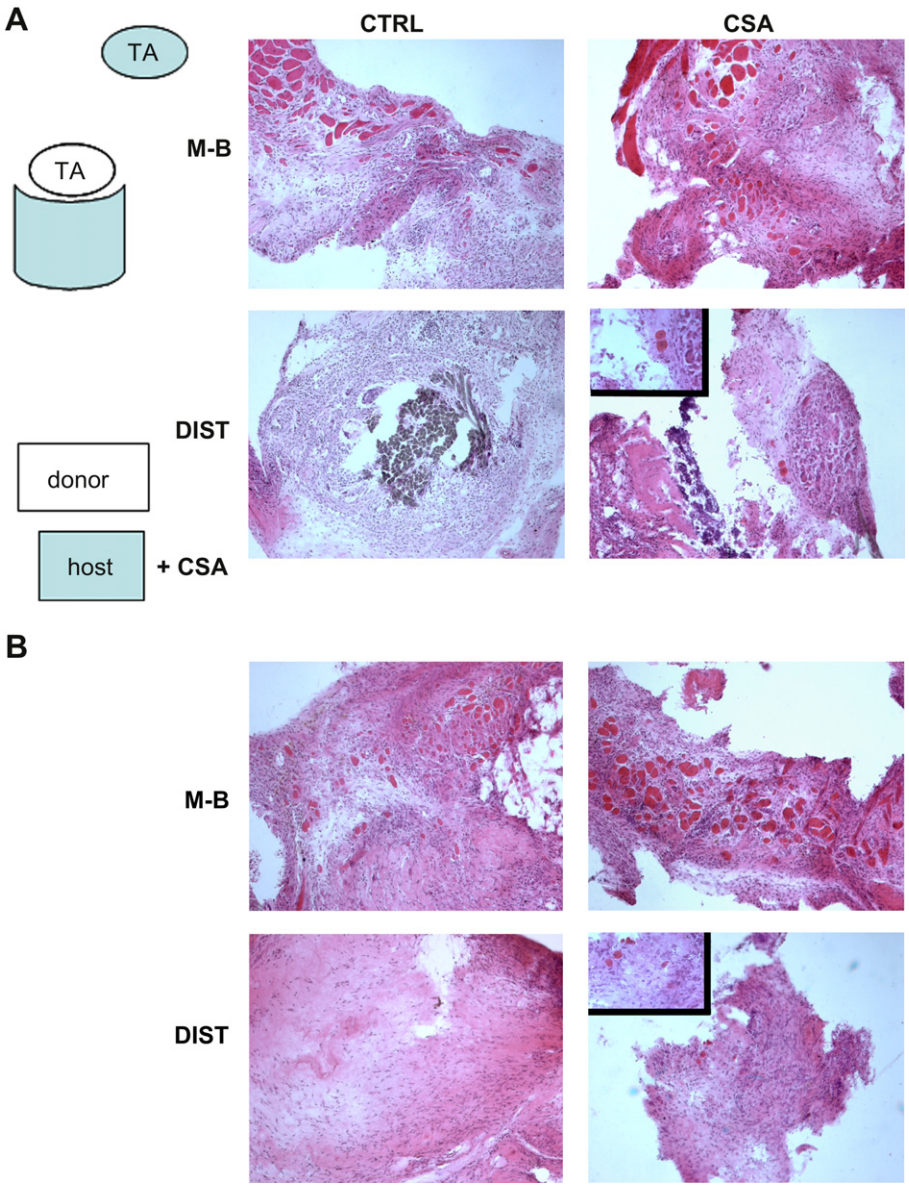

Fig. 8. Host–donor tissue integration upon immunosuppression. The diagram depicts the experimental procedure, consisting in host TA (blue) removal, followed by orthotopic transplantation of a TA acellular scaffold (white) upon daily treatment with CSA or vehicle (CTRL), as described in M&M. Reconstruction of a whole graft cryosection at the mid-belly (M-B) and in the distal (DIST) region, at the three-week (A) and four-week (B) time points, obtained by merging a series of high definition images of H&E stained samples. The insets show 40× magnification of the image. The histological analysis indicates that the grafts are stable for up to four weeks following transplantation, during which they display regenerating myofibers and resorption is absent. In addition, we observed that, in the presence of CSA treatment, regenerating myofibers were more numerous and extended to the distal end of the construct, which was in sharp contrast to the controls. (For interpretation of the references to colour in this figure legend, the reader is referred to the web version of this article.)

presence of laminin is due to neo-secretion and remodeling performed by the host cells in the grafted material. CSA selectively inhibits T-helper cell production of growth factors required for B cell and cytotoxic T-cell differentiation and proliferation [26]. In addition, cyclosporine inhibits macrophage-mediated antigen presentation [34]. Nude mice can receive numerous types of xenografts, as their rejection response is either absent or reduced owing to the absence of a functional thymus [35]. Immunosuppressive treatments, such as CSA, affect scaffold integration and bioactivity, resulting in increased myogenesis. However, we observed comparable responses to allografted scaffolds in wt and nude (i.e. T-cell defective) mice. Taken together, our results suggest that it is macrophages, as opposed to T lymphocytes, that play a major role in acellular muscle graft integration.

The mononucleated cells that invade the grafted material include potentially myogenic stem cells, i.e. PW1 expressing cells or PICs [22]. Previous studies have reported both the migration of mesenchymal stem cells to heart allografts during chronic rejection and their contribution to cardiac repair [36,37]. In skeletal muscle, satellite cells, which are muscle fiber attendant cells, are primarily responsible for fiber generation and repair. Previous studies by us and other researchers have, however, also reported that myogenic resident stem cells are involved in muscle postnatal growth and regeneration following injury [15,22,23]. In addition, non-muscle stem cells can migrate toward regenerating muscle and participate in skeletal muscle repair [38]. We hypothesize that PICs, and possibly other myogenic cells, colonize the graft and are induced to differentiate into multinucleated myofibers. Indeed, the presence of

nascent muscle fibers in the grafted materials is probably the most striking finding of our research. Even though we do not directly demonstrate the contribution of host cells to these newly formed fibers, it is likely that the ECM from skeletal muscle constitutes a pro-myogenic environment that is sufficient *per se* to induce host stem cells to myogenic differentiation. To the best of our knowledge, this is the first time allografted ECM derived from decellularized skeletal muscle has been reported to promote myogenesis *in vivo*. Other groups have shown that either minced or whole skeletal muscle can completely regenerate when autografted in wt mice [11,39], and that heterologous muscle acellular matrix seeded with autologous myoblasts can be exploited for patch repairs [10]. However, it is difficult to obtain autologous tissue components because of the limited availability of autologous donor tissue from a patient. It was, therefore, important to characterize the host response to an acellular scaffold of allogenic origin and to demonstrate that the ECM component of a muscle allograft itself recruits and induces host cells to differentiate. Since no cells survived the SDS treatment used to produce transplantable scaffolds in our experimental setting, we may infer that the neo-myogenesis that occurred within the graft was due to host-derived infiltrating myogenic cells. This hypothesis is supported by previous findings showing that regeneration within a grafted muscle is enhanced when stem cell activation is induced in the surrounding muscles [40]. This last result indicates that the musculature surrounding an implant is a potential source of myoblasts capable of invading the graft and promoting myogenesis. A growing body of evidence has highlighted the pivotal importance of the niche to the regulation of stem cell function not only in skeletal muscle [16], but in other tissues as well [41]. Our results indicate that skeletal muscle ECM scaffolds represent a favorable environment for the neoformation of skeletal muscle *in vivo*, suggesting that they posses muscle niche properties.

Procedures designed to exploit and enhance skeletal muscle ECM as a biomaterial are readily translating to regenerative medicine applications [42–45]. Our results together with those of others [43,45] show that ECM of various origin can efficiently be used to reconstruct skeletal muscle tissue morphologically and functionally similar to naïve muscle. The main differences with similar studies reside in the fact that Badylak and co-workers used other animal models (rats or dogs) in respect to our model (mice), and essentially ECM from other tissues to repair muscle or musculo-tendinous defects [43,45]. In some cases transplanted muscle tissue was used to repair a muscle defect, i.e. a patch of complete tissue was used, as opposed to our approach where only the muscle ECM was grafted [43]. Thus, our approach adds additional values to this study, since it suggests that it is the ECM, and not the cellular component, of the muscle tissue to have pro-myogenic properties. An advantage of using acellular ECM scaffold as opposed to tissue patch is that acellular scaffold can be stored at $+4\,^{\circ}C$ for a more significant time in respect to tissues. All these considerations will significantly affect the development of off-the-shelf products for future interventions in regenerative medicine. The successful translation of tissue-engineered constructs into everyday clinical practice will also depend upon the ability to scale up every aspect of the research and development process. A critical issue in the translatability of acellular scaffold grafts remains the repopulation by human cells *in vivo*. However, it has been recently reported that human cells were able to participate in muscle regeneration and scaffold-implanted muscles of nude mice [46]. For what concern other tissues, human dental pulp stem cells have been shown to repopulate scaffolds *in vivo*, ultimately leading to odontogenic differentiation [47]. Most of these studies showing human stem cell repopulation of scaffold were performed in nude mice host. However, scaffolds and skin substitutes are efficiently repopulated *in vivo* and are currently used in clinical practice, indicating the feasibility of the use of scaffolds that are repopulated by endogenous or transplanted cells in humans [48].

5. Conclusion

Allografts of acellular scaffold derived from a whole skeletal muscle explanted from mice and orthotopically transplanted in wt mice remain stable for several weeks, whilst being colonized by inflammatory and stem cells. Acellular scaffolds *per se* represent a pro-myogenic environment supporting *de novo* formation of muscle fibers, likely derived from host cells with myogenic potential. Inflammation by immunosuppressive procedures increases the volume of skeletal muscle fibers, thereby improving the outcome of the graft. Our work highlights the role this niche plays in TE applications and unveils the clinical potential of allografts based on decellularized tissue in regenerative medicine.

Acknowledgments

We gratefully acknowledge the technical help provided by Carla Ramina and Fabrizio Padula (Sapienza University of Rome) for the confocal and flow cytometry analysis, respectively. We thank Giovanna Marazzi and David Sassoon, who have provided the 370 (anti-PW1) Ab. The authors are also grateful to Dario Rossi for his multimedia advice and expertise. Grant support from the following institution is acknowledged: AFM, Italian MIUR, Sapienza University of Rome to SA; UPMC Emergence to DC.

Appendix. Supplementary material

Supplementary data associated with this article can be found in the online version, at doi:10.1016/j.biomaterials.2011.07.016.

References

[1] Williams DF. On the nature of biomaterials. Biomaterials 2009;30:5897–909.
[2] Qing Q, Qin T Optimal method for rat skeletal muscle decellularization. Zhongguo Xiu Fu Chong Jian Wai Ke Za Zhi 2009;23:836–9.
[3] Chen RN, Ho HO, Tsai YT, Sheu MT. Process development of an acellular dermal matrix (ADM) for biomedical applications. Biomaterials 2004;25:2679–86.
[4] Ketchedjian A, Jones AL, Krueger P, Robinson E, Crouch K, Wolfinbarger Jr L, et al. Recellularization of decellularized allograft scaffolds in ovine great vessel reconstructions. Ann Thorac Surg 2005;79:888–96.
[5] Ott HC, Matthiesen TS, Goh SK, Black LD, Kren SM, Netoff TI, et al. Perfusion-decellularized matrix: using nature's platform to engineer a bioartificial heart. Nat Med 2008;14:213–21.
[6] Badylak SF. The extracellular matrix as a biologic scaffold material. Biomaterials 2007;28:3587–93.
[7] Martinez FO, Sica A, Mantovani A, Locati M. Macrophage activation and polarization. Front Biosci 2008;13:453–61.
[8] Klumpp D, Horch RE, Kneser U, Beier JP. Engineering skeletal muscle tissue–new perspectives in vitro and in vivo. J Cell Mol Med 2010;14:2622–9.
[9] Borschel GH, Dennis RG, Kuzon Jr WM. Contractile skeletal muscle tissue-engineered on an acellular scaffold. Plast Reconstr Surg 2004;113:595–602.
[10] Conconi MT, De Coppi P, Bellini S, Zara G, Sabatti M, Marzaro M, et al. Homologous muscle acellular matrix seeded with autologous myoblasts as a tissue-engineering approach to abdominal wall-defect repair. Biomaterials 2005;26:2567–74.
[11] Bierinx AS, Sebille A. Mouse sectioned muscle regenerates following autografting with muscle fragments: a new muscle precursor cells transfer? Neurosci Lett 2008;431:211–4.
[12] Macri L, Silverstein D, Clark RA. Growth factor binding to the pericellular matrix and its importance in tissue engineering. Adv Drug Deliv Rev 2007;59:1366–81.
[13] Grounds MD, Radley HG, Lynch GS, Nagaraju K, De Luca A. Towards developing standard operating procedures for pre-clinical testing in the mdx mouse model of Duchenne muscular dystrophy. Neurobiol Dis 2008;31:1–19.
[14] Stern MM, Myers RL, Hammam N, Stern KA, Eberli D, Kritchevsky SB, et al. The influence of extracellular matrix derived from skeletal muscle tissue on the proliferation and differentiation of myogenic progenitor cells ex vivo. Biomaterials 2009;30:2393–9.

[15] Moresi V, Garcia-Alvarez G, Pristera A, Rizzuto E, Albertini MC, Rocchi M, et al. Modulation of caspase activity regulates skeletal muscle regeneration and function in response to vasopressin and tumor necrosis factor. PloS One 2009; 4:e5570.
[16] Pelosi L, Giacinti C, Nardis C, Borsellino G, Rizzuto E, Nicoletti C, et al. Local expression of IGF-1 accelerates muscle regeneration by rapidly modulating inflammatory cytokines and chemokines. Faseb J 2007;21:1393–402.
[17] De Arcangelis V, Coletti D, Conti M, Lagarde M, Molinaro M, Adamo S, et al. IGF-I-induced differentiation of L6 myogenic cells requires the activity of cAMP-phosphodiesterase. Mol Biol Cell 2003;14:1392–404.
[18] Liao IC, Leong KW. Efficacy of engineered FVIII-producing skeletal muscle enhanced by growth factor-releasing co-axial electrospun fibers. Biomaterials 2011;32:1669–77.
[19] Lim DG, Koo SK, Park YH, Kim Y, Kim HM, Park CS, et al. Impact of immunosuppressants on the therapeutic efficacy of in vitro-expanded CD4+CD25+Foxp3+ regulatory T cells in allotransplantation. Transplantation 2010;89:928–36.
[20] Davis BJ. Histochemical demonstration of erythrocyte esterases. Proc Soc Exp Biol Med 1959;101:90–3.
[21] Berardi E, Aulino P, Murfuni I, Toschi A, Padula F, Scicchitano BM, et al. Skeletal muscle is enriched in hematopoietic stem cells and not inflammatory cells in cachectic mice. Neurol Res 2008;30:160–9.
[22] Mitchell KJ, Pannerec A, Cadot B, Parlakian A, Besson V, Gomes ER, et al. Identification and characterization of a non-satellite cell muscle resident progenitor during postnatal development. Nat Cell Biol 2010;12:257–66.
[23] Moresi V, Pristera A, Scicchitano BM, Molinaro M, Teodori L, Sassoon D, et al. Tumor necrosis factor-alpha inhibition of skeletal muscle regeneration is mediated by a caspase-dependent stem cell response. Stem Cells 2008;26: 997–1008.
[24] Aulino P, Berardi E, Cardillo VM, Rizzuto E, Perniconi B, Ramina C, et al. Molecular, cellular and physiological characterization of the cancer cachexia-inducing C26 colon carcinoma in mouse. BMC Cancer 2010;10:363.
[25] Liu H, Wang Y, Li S. Advanced delivery of ciclosporin A: present state and perspective. Expert Opin Drug Deliv 2007;4:349–58.
[26] Cohen DJ, Loertscher R, Rubin MF, Tilney NL, Carpenter CB, Strom TB. Cyclosporine: a new immunosuppressive agent for organ transplantation. Ann Intern Med 1984;101:667–82.
[27] Lu H, Hoshiba T, Kawazoe N, Chen G. Autologous extracellular matrix scaffolds for tissue engineering. Biomaterials 2011;2:2489–99.
[28] Lutolf MP, Hubbell JA. Synthetic biomaterials as instructive extracellular microenvironments for morphogenesis in tissue engineering. Nat Biotechnol 2005;23:47–55.
[29] Carlson EC, Carlson BM. A method for preparing skeletal muscle fiber basal laminae. Anat Rec (Hoboken) 1991;230:325–31.
[30] Badylak SF, Gilbert TW. Immune response to biologic scaffold materials. Semin Immunol 2008;20:109–16.
[31] Schenke-Layland K, Vasilevski O, Opitz F, Konig K, Riemann I, Halbhuber KJ, et al. Impact of decellularization of xenogeneic tissue on extracellular matrix integrity for tissue engineering of heart valves. J Struct Biol 2003;143:201–8.
[32] Bartholomew A, Sturgeon C, Siatskas M, Ferrer K, McIntosh K, Patil S, et al. Mesenchymal stem cells suppress lymphocyte proliferation in vitro and prolong skin graft survival in vivo. Exp Hematol 2002;30:42–8.
[33] Li F, Li W, Johnson S, Ingram D, Yoder M, Badylak S. Low-molecular-weight peptides derived from extracellular matrix as chemoattractants for primary endothelial cells. Endothelium 2004;11:199–206.
[34] Palay DA, Cluff CW, Wentworth PA, Ziegler HK. Cyclosporine inhibits macrophage-mediated antigen presentation. J Immunol 1986;136:4348–53.
[35] Matsunuma H, Kagami H, Narita Y, Hata K, Ono Y, Ohshima S, et al. Constructing a tissue-engineered ureter using a decellularized matrix with cultured uroepithelial cells and bone marrow-derived mononuclear cells. Tissue Eng 2006;12:509–18.
[36] Wu GD, Bowdish ME, Jin YS, Zhu H, Mitsuhashi N, Barsky LW, et al. Contribution of mesenchymal progenitor cells to tissue repair in rat cardiac allografts undergoing chronic rejection. J Heart Lung Transplant 2005;24:2160–9.
[37] Wu GD, Nolta JA, Jin YS, Barr ML, Yu H, Starnes VA, et al. Migration of mesenchymal stem cells to heart allografts during chronic rejection. Transplantation 2003;75:679–85.
[38] Yang R, Chen M, Lee CH, Yoon R, Lal S, Mao JJ. Clones of ectopic stem cells in the regeneration of muscle defects in vivo. PloS One 2010;5:e13547.
[39] Smythe GM, Grounds MD. Exposure to tissue culture conditions can adversely affect myoblast behavior in vivo in whole muscle grafts: implications for myoblast transfer therapy. Cell Transplant 2000;9:379–93.
[40] Vindigni V, Mazzoleni F, Rossini K, Fabbian M, Zanin ME, Bassetto F, et al. Reconstruction of ablated rat rectus abdominis by muscle regeneration. Plast Reconstr Surg 2004;114:1509–15.
[41] Ferraro F, Celso CL, Scadden D. Adult stem cells and their niches. Adv Exp Med Biol 2010;695:155–68.
[42] Hall JK, Banks GB, Chamberlain JS, Olwin BB. Prevention of muscle aging by myofiber-associated satellite cell transplantation. Sci Transl Med 2010;2. 57ra83.
[43] Valentin JE, Turner NJ, Gilbert TW, Badylak SF. Functional skeletal muscle formation with a biologic scaffold. Biomaterials 2010;31:7475–84.
[44] Rustad KC, Sorkin M, Levi B, Longaker MT, Gurtner GC. Strategies for organ level tissue engineering. Organogenesis 2010;6:151–7.
[45] Turner NJ, Yates Jr AJ, Weber DJ, Qureshi IR, Stolz DB, Gilbert TW, et al. Xenogeneic extracellular matrix as an inductive scaffold for regeneration of a functioning musculotendinous junction. Tissue Eng Part A 2010;16: 3309–17.
[46] Boldrin L, Malerba A, Vitiello L, Cimetta E, Piccoli M, Messina C, et al. Efficient delivery of human single fiber-derived muscle precursor cells via biocompatible scaffold. Cell Transplant 2008;17:577–84.
[47] Wang J, Ma H, Jin X, Hu J, Liu X, Ni L, et al. The effect of scaffold architecture on odontogenic differentiation of human dental pulp stem cells. Biomaterials; 2011 [Epub ahead of print].
[48] Pham C, Greenwood J, Cleland H, Woodruff P, Maddern G. Bioengineered skin substitutes for the management of burns: a systematic review. Burns 2007; 33:946–57.